Electronic Supplementary Material (ESI) for Journal of Materials Chemistry A.
This journal is © The Royal Society of Chemistry 2019

Supporting information

Low-Temperature Electroless Synthesis of Mesoporous Aluminum Nanoparticles on Graphene for High-Performance Lithium-Ion Batteries

Hongyu Zhang,[a] Guanglin Xia,*[ab] Fang Fang,[a] Dalin Sun[a] and Xuebin Yu, *[a]

[a]Department of Materials Science, Fudan University, Shanghai 200433, China

[b]Institute for Superconducting and Electronic Materials, University of Wollongong, North Wollongong, NSW 2522, Australia

*Corresponding authors

*E-mail: xiaguanglin@fudan.edu.cn; yuxuebin@fudan.edu.cn

Experimental Section:

All samples were prepared in an argon purified glove box (MBraun Labmaster) with moisture and oxygen levels below 0.1 ppm.

Synthesis of Mg@G: MgH_2 nanoparticles uniformly dispersed on graphene were first prepared through the hydrogenation-induced self-assembly method described in our previous report[4]. Typically, 1.7 mL of $MgBu_2$ solution (1 M in heptane) and 0.02 g of graphene were mixed in a pressure reactor vessel under ultrasonic treatment for 1 h. Subsequently, the mixture was heated at 220 ^oC under a hydrogen pressure of 2 MPa with a heating rate of 2 $^oC\ min^{-1}$. After drying under dynamic vacuum on a Schlenk line, the obtained MgH_2 nanoparticles distributed on graphene were dehydrogenated to obtain Mg@G.

Electroless synthesis of mp-Al@G: Typically, to ensure the complete reaction between Mg and $AlCl_3$, 0.02 g of Mg@G was first mixed with 0.07 g of anhydrous $AlCl_3$ (99.99 %) with a stoichiometric ratio of 1:1 through ball milling (Fig. S28) and the mixture was then transferred into a sealed pressure reaction vessel and heated at 190 ^oC for 6 h. After consecutive washing and centrifugation with anhydrous tetrahydrofuran (THF, 99.9 %), the composite was dried under dynamic vacuum at 80 ^oC on a Schlenk line to obtain the mesoporous Al nanoparticles dispersed on graphene (mp-Al@G).

Synthesis of BM Al-G: Commercial Al NPs and graphene in a gravimetric ratio of 4:6 (according to the weight ratio between mesoporous Al NPs and graphene in mp-Al@G) were uniformly mixed

via ball milling at 350 rpm for 6 h to obtain BM Al-G using a planetary QM-1SP2.

Characterizations: The phase composition of the as-prepared samples was measured by X-ray diffraction (XRD, D8 Advance, Bruker AXS Corporation) with Cu Kα radiation (λ = 1.5418 Å). The morphology of the samples was obtained with a transmission electron microscope (TEM; JEOL 2011 F, Tokyo, Japan) and a field emission scanning electron microscope (FE-SEM; JEOL 7500FA, Tokyo, Japan). Thermogravimetric analysis (TG, Netzsch STA449 F3) was performed under an air flow rate of 80 ml min^{-1} with a heating rate of 10 ^{o}C min^{-1}. The Raman spectrum of the as-synthesized mp-Al@G was collected using a Fourier-transform infrared Raman spectrometer (NEXUS 670). The nitrogen absorption-desorption isotherms of the samples were collected using a Quantachrome NOVA 4200e instrument at the temperature of liquid nitrogen. The specific surface area and pore size distribution were analyzed through the Brunauer–Emmett–Teller (BET) and Barrett-Joyner-Halenda (BJH) models. X-ray photoemission spectroscopy (XPS) experiments were performed on a Perkin Elmer PHI 5000C ESCA system with a dual X-ray source, using an Mg Kα (1253.6 eV) anode with a hemispherical energy analyzer. The background pressure was kept at < 10^{-6} Pa during data acquisition, and measurements were carried out at a pass energy of 93.90 eV. All binding energies were calibrated by using the contaminant carbon (C 1s = 284.6 eV) as a reference.

Fabrication of electrodes: The mp-Al@G electrode was prepared by mixing the active materials (70 wt.%), Super P carbon black (20 wt.%), and polyvinylidene fluoride (PVDF) (10 wt.%) in N-methyl pyrrolidone (NMP) to obtain a uniform slurry. Subsequently, the slurry was pasted on copper foil.

The $LiNi_{0.6}Co_{0.2}Mn_{0.2}O_2$ (NCM) electrode was prepared by mixing the active materials, Super P carbon black, and PVDF in a ratio of 8:1:1 in NMP, and the obtained slurry was then pasted on Al foil. After weighing, both electrodes were further dried at 80 ^oC for 24 h under vacuum before coin cell assembly. For half cells, mp-Al@G and/or $LiNi_{0.6}Co_{0.2}Mn_{0.2}O_2$ electrode were employed as the working electrode, pure lithium foil was used as both the counter electrode and the reference electrode, and a Celgard 2400 membrane was used as the separator. The electrolyte was 1 M $LiPF_6$ dissolved in ethyl carbonate (EC) and dimethyl carbonate (DMC) (1/1; v/v) with the addition of 5 wt.% fluoroethylene carbonate (FEC). For the mp-Al@G//NCM full cells, the electrolytes and separators were the same as those used in the half cells. The mp-Al@G electrode was first activated in a half cell for 2 cycles and then taken out to act as the anode for the full cells and the $LiNi_{0.6}Co_{0.2}Mn_{0.2}O_2$ electrode was directly used as the cathode. The typical capacity ratio between anode and cathode was 1.1:1. The mass loading of mp-Al@G electrode and $LiNi_{0.6}Co_{0.2}Mn_{0.2}O_2$ electrode was around 1.1 mg cm^{-2} and 5.9 mg cm^{-2}, respectively. All electrochemical measurements were performed using CR2032-type coin cells, and the coin cells were sealed in a manual hydraulic crimping machine (MSK – 110, MTI Corporation).

Electrochemical characterizations: The galvanostatic charge/discharge measurements of half cells and the mp-Al@G//NCM full cells were performed on a LAND battery testing system at room temperature. The voltage cut-off window was 0.01 - 3 V for the mp-Al@G electrode in half cells, 2.7 – 4.5 V for the NMC electrode in half cells, and 2.4 – 4.4 V for full cells. The cyclic voltammetry (CV) measurements of mp-Al@G electrode in half cells were conducted in the voltage range of 0.01 - 3 V at the scan rates of 0.1, 0.2, 0.3, and 0.8 mV s^{-1}, and the electrochemical impedance

spectroscopy (EIS) tests were performed in the frequency range from 100 kHz to 0.01 Hz on an electrochemical workstation (CHI 660E). All current density and specific capacity calculations were based on the total mass of the active materials (mesoporous Al and graphene, or $LiNi_{0.6}Co_{0.2}Mn_{0.2}O_2$) for half cells, and the applied current density of 1 C in the full cell tests equals 0.26 A g^{-1}. In the digital image of 29 red LEDs lit by three mp-Al@G//NCM full cells, the lights in direction of the green arrow are in parallel and then they are in series in direction of the black arrow.

Calculation of the capacitive contribution: The capacitive contribution to the current response at different scan rates is subsequently calculated according to[1-3]:

$$i\,(V) = k_1\,v + k_2\,v^{1/2}$$

where i is the current response, v is the scan rate, V is the fixed voltage, $k_1\,v$ is the capacitive contribution, and $k_2\,v^{1/2}$ is the surface-controlled contribution. By determining k_1 and k_2, the fraction of capacitive and diffusion-controlled contribution could be quantified.

Calculation of energy density: Generally, the total mass of mp-Al@G and $LiNi_{0.6}Co_{0.2}Mn_{0.2}O_2$ was used to calculate the specific capacity of the full cell. Therefore, the energy density ($E_{full\text{-}cell}$) based on the total mass of active materials (*i.e.,* mp-Al@G and $LiNi_{0.6}Co_{0.2}Mn_{0.2}O_2$) could be calculated according to the equation as shown below[5-7]:

$$E_{full\text{-}cell} = C_{(anode\,+\,cathode)} \times V_{nominal}$$

where $V_{nominal}$ is the average voltage and $C_{(anode\,+\,cathode)}$ is the specific capacity of the assembled full-cells based on the total weight of anode and cathode materials.

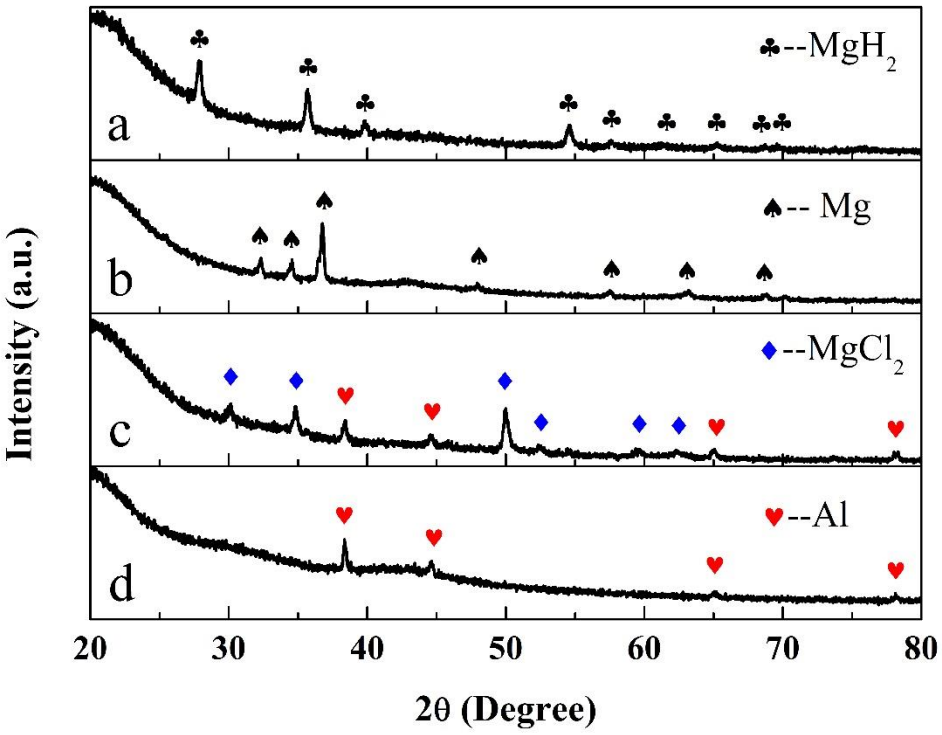

Figure S1 XRD patterns of a) MgH_2@G, b) Mg@G, c) the reaction product of ball-milled $AlCl_3$ + Mg@G composite after heat treatment, and d) the as-synthesized mp-Al@G.

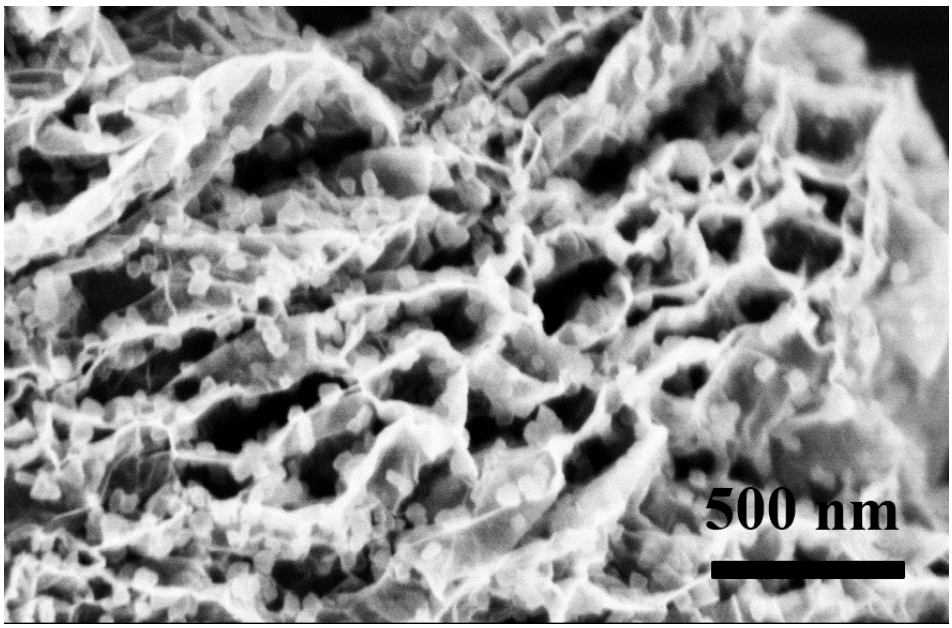

Figure S2 Cross-sectional SEM image of Mg@G.

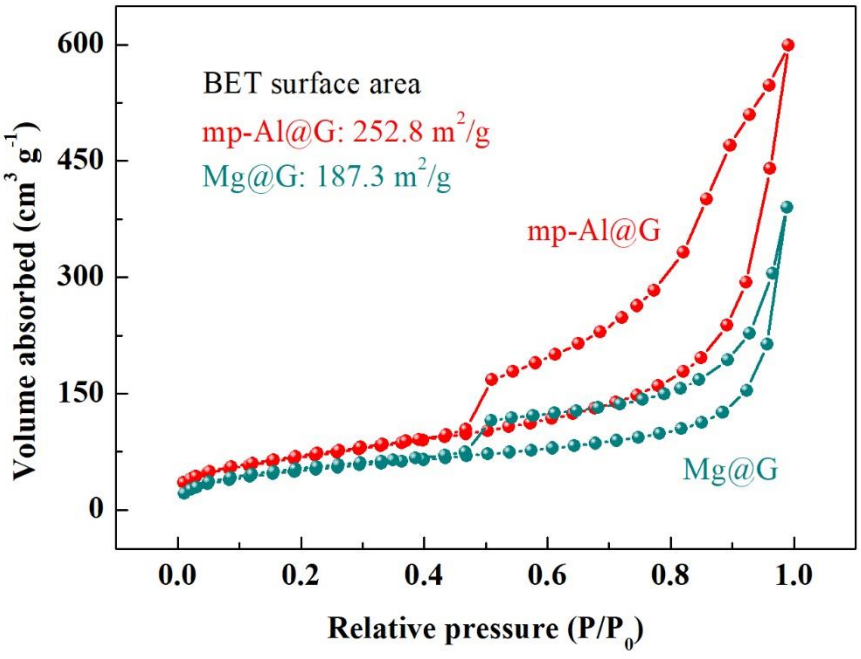

Figure S3 Nitrogen adsorption/desorption isotherms and BET surface areas of mp-Al@G and Mg@G.

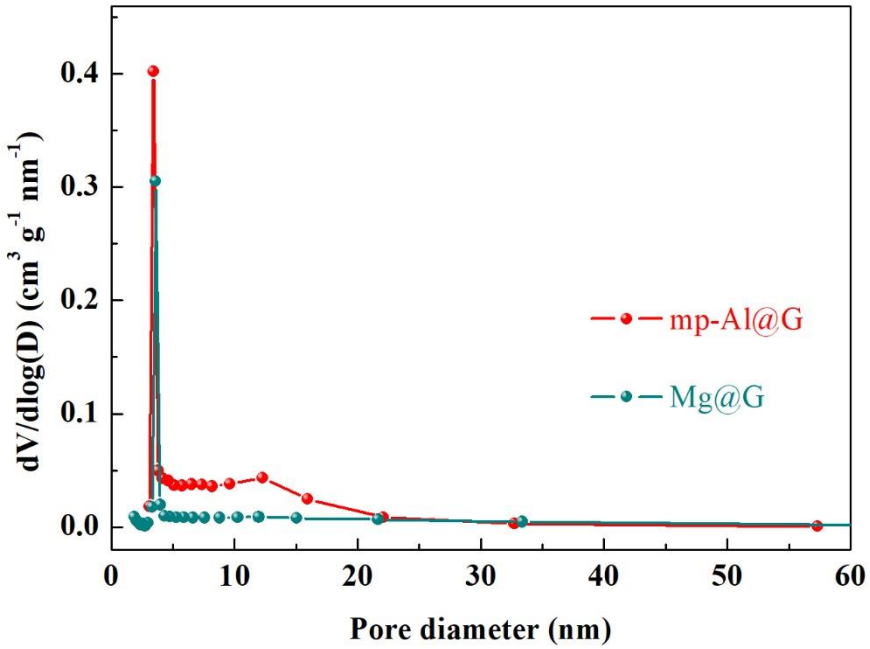

Figure S4 The pore-size distributions of mp-Al@G and Mg@G.

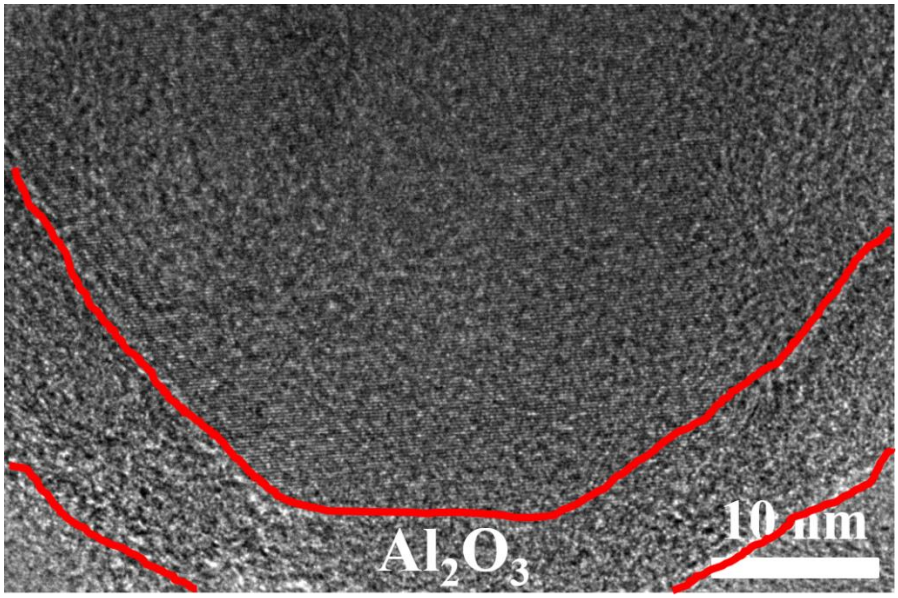

Figure S5 TEM image of commercial Al NP with the obvious presence of an amorphous oxide layer.

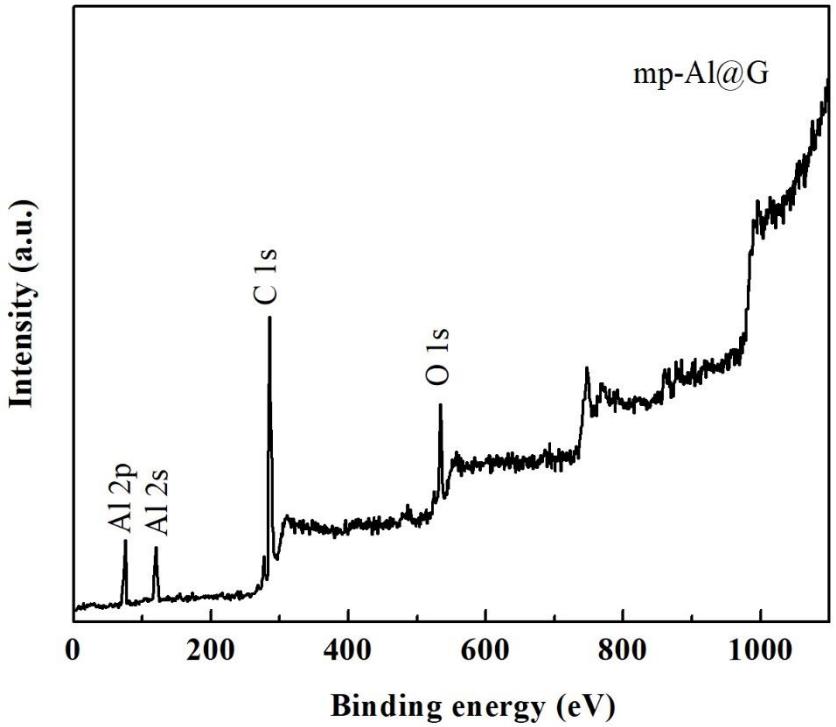

Figure S6 XPS survey spectrum of the as-synthesized mp-Al@G.

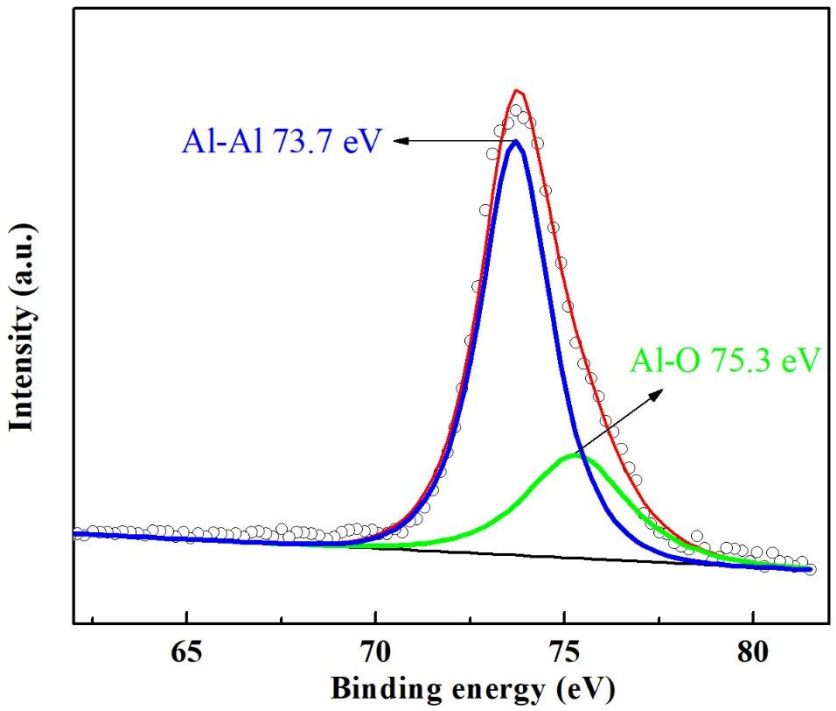

Figure S7 High-resolution Al 2p spectrum of mp-Al@G.

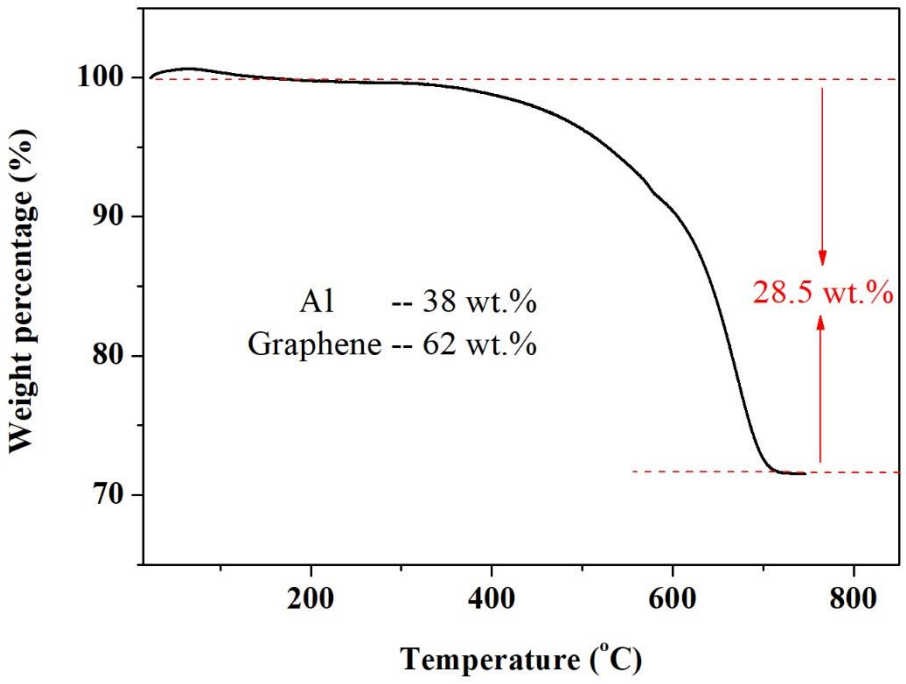

Figure S8 TGA curve of mp-Al@G under air.

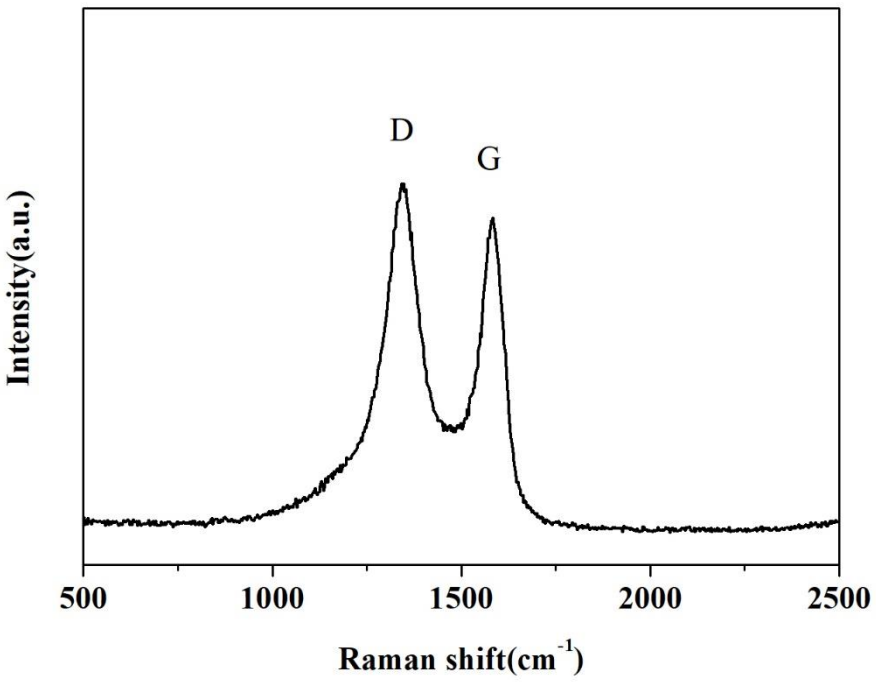

Figure S9 Raman spectrum of mp-Al@G.

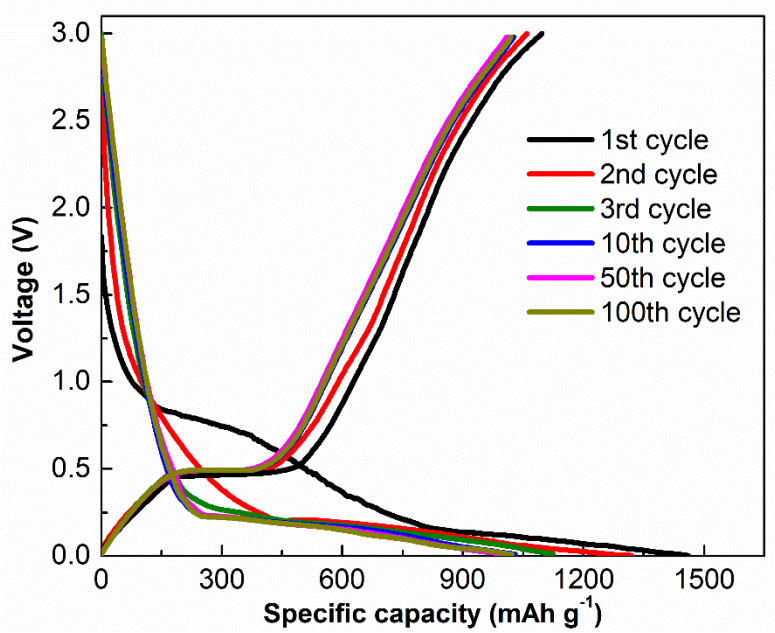

Figure S10 The detailed galvanostatic charge-discharge curves of mp-Al@G for the 1st, 2nd, 3rd, 10th, 50th, and 100th cycle at 0.2 A g^{-1}.

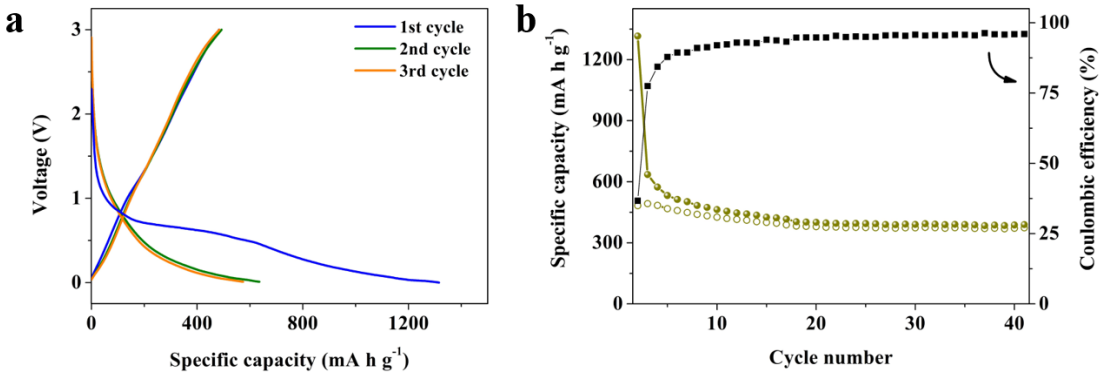

Figure S11 (a) The detailed galvanostatic charge-discharge curves and (b) cycling performance of graphene obtained from mp-Al@G after etching of mp-Al at 0.2 A g^{-1}.

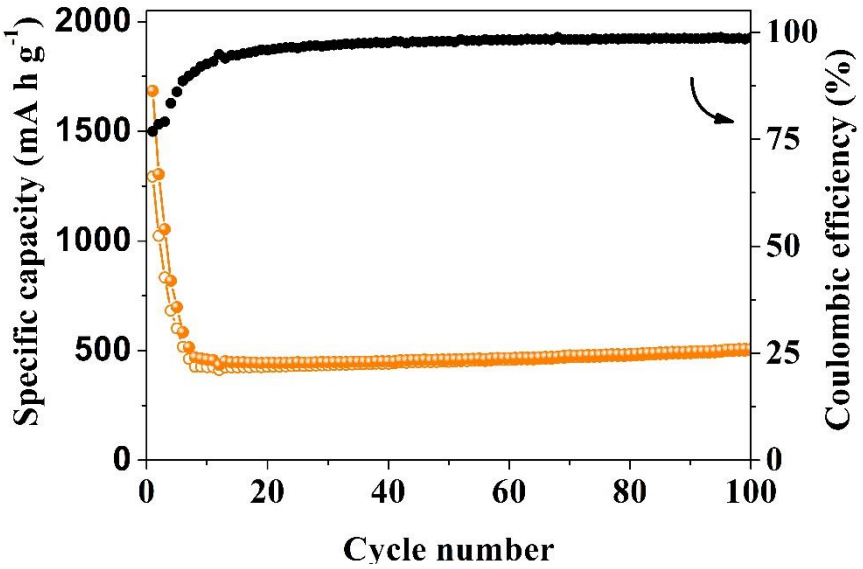

Figure S12 Cycling performance and Coulombic efficiency of mp-Al@G with Al content of 75 wt.% at 0.2 A g^{-1}.

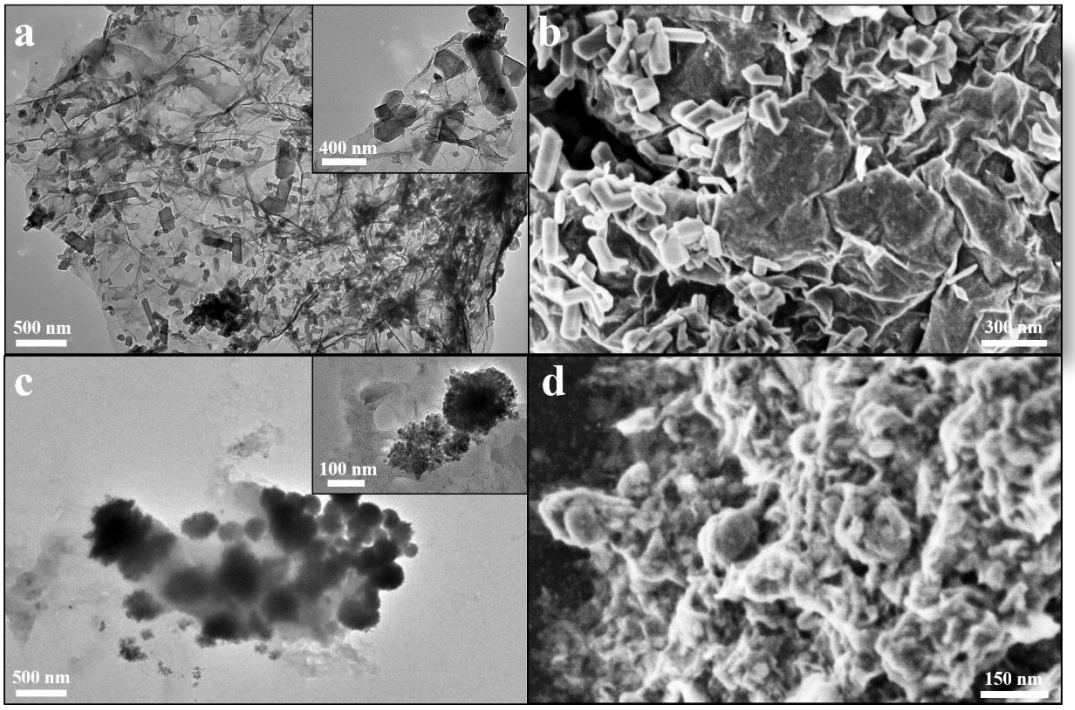

Figure S13 (a) TEM and (b) SEM images of Mg@G with a loading ratio of 80%, (c) TEM and (d) SEM images of the as-synthesized mp-Al@G with a loading ratio of 70%. The insets of a and c are the magnified TEM images of Mg@G and mp-Al@G, respectively.

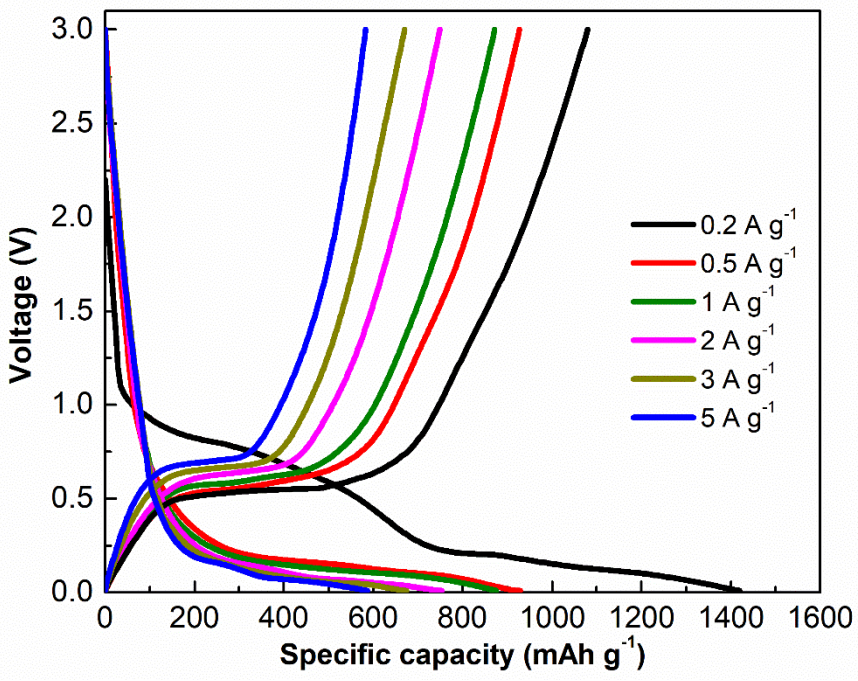

Figure S14 Galvanostatic charge-discharge curves of mp-Al@G at 0.2 A g^{-1}, 0.5 A g^{-1}, 1 A g^{-1}, 2 A g^{-1}, 3 A g^{-1}, and 5 A g^{-1}, respectively

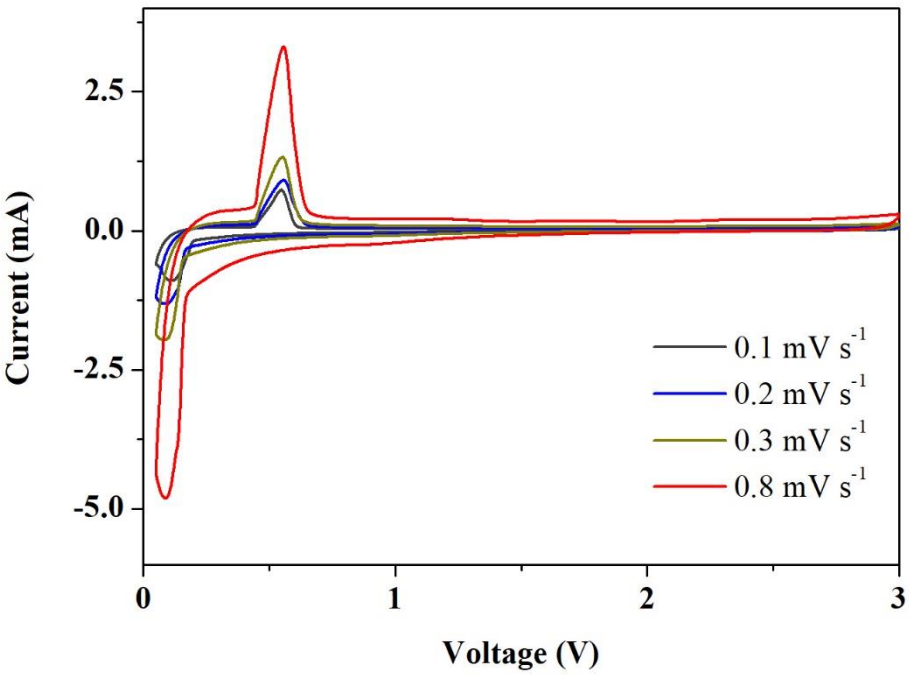

Figure S15. CV curves of mp-Al@G at different scan rates.

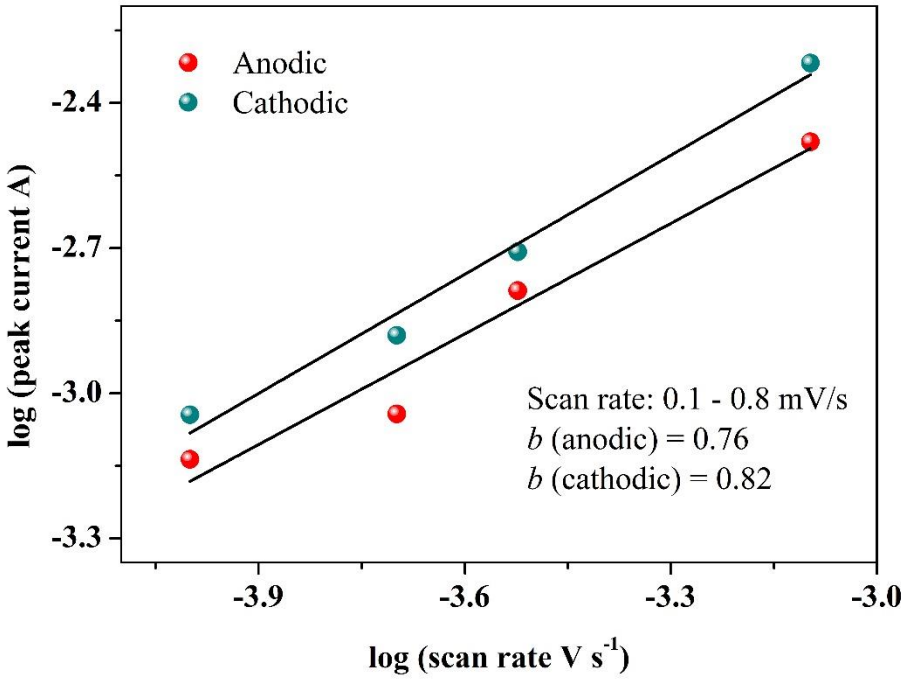

Figure S16. *b*-values for the cathodic and anodic peaks of mp-Al@G.

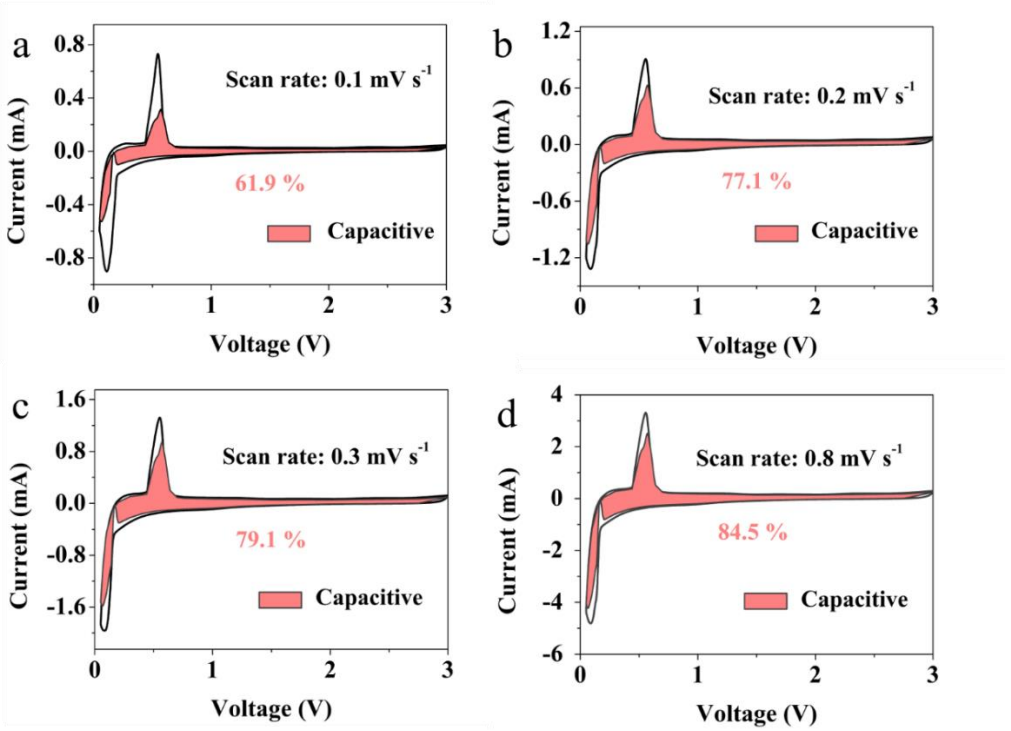

Figure S17. The capacitive contributions to the capacity of mp-Al@G at the scan rates of a) 0.1, b) 0.2, c) 0.3, and d) 0.8 mV s^{-1}.

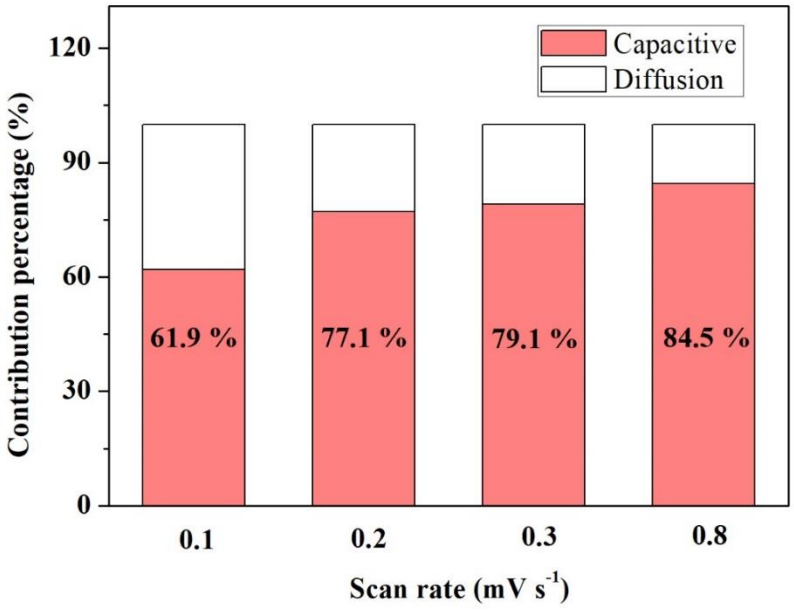

Figure S18. Normalized contribution ratios of capacitive and diffusion-controlled capacities at different scan rates.

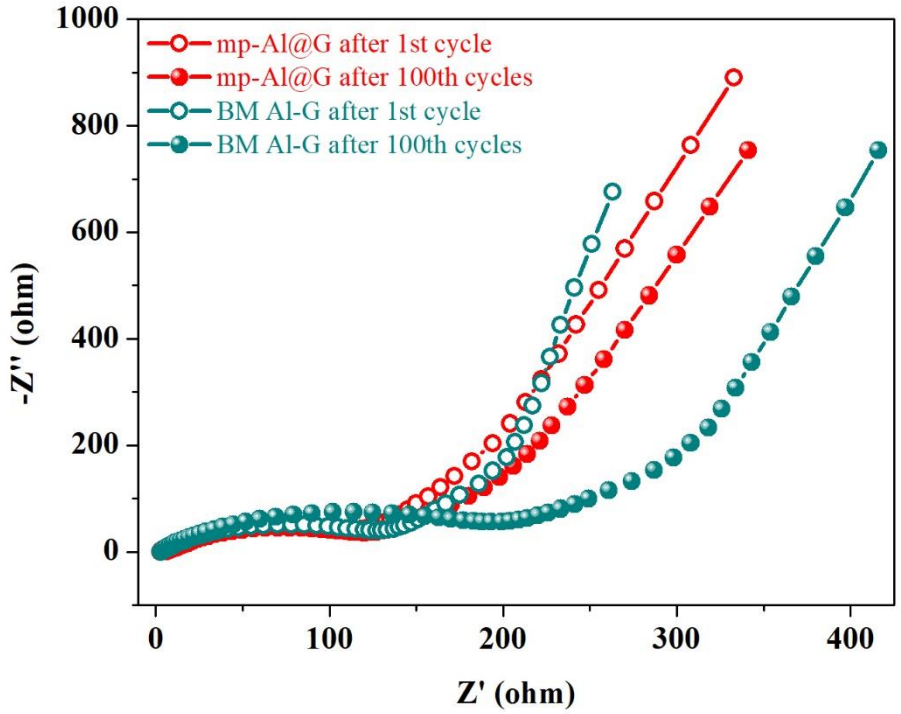

Figure S19 Nyquist plots of mp-Al@G and BM Al-G after the 1st and the 100th cycles.

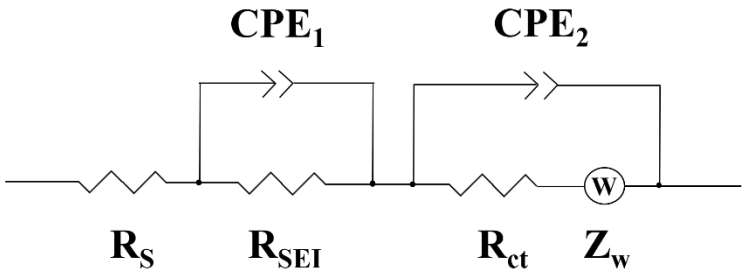

Figure S20 The corresponding equivalent circuit model for fitting the EIS spectra (R_S, R_{SEI}, R_{ct}, CPE, and Z_w refer to the internal resistance, surface layer resistance, charge transfer resistance, constant phase elements, and Warburg impedance of the tested battery, respectively.)

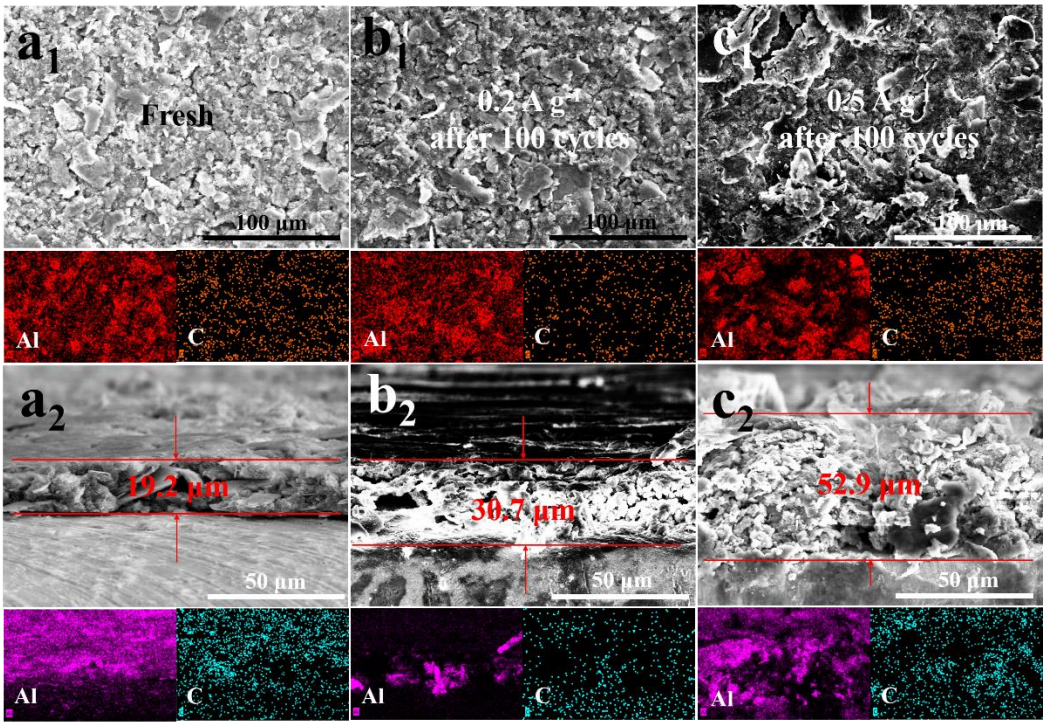

Figure S21 SEM images and the corresponding element mappings of commercial Al NPs electrode in various states: (a_1, a_2) fresh, (b_1, b_2) after 100 cycles at 0.2 A g^{-1}, and (c_1, c_2) after 100 cycles at 0.5 A g^{-1}.

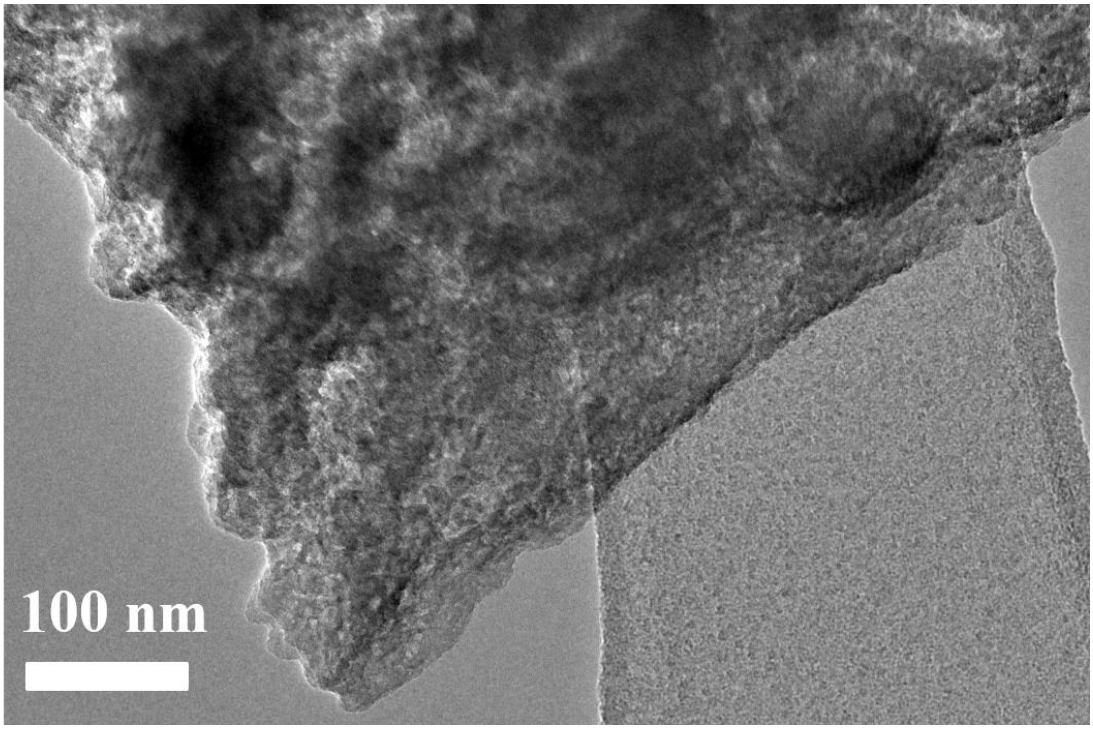

Figure S22 TEM image of mp-Al@G electrode after 100 cycles at a current density of 0.5 A g^{-1}.

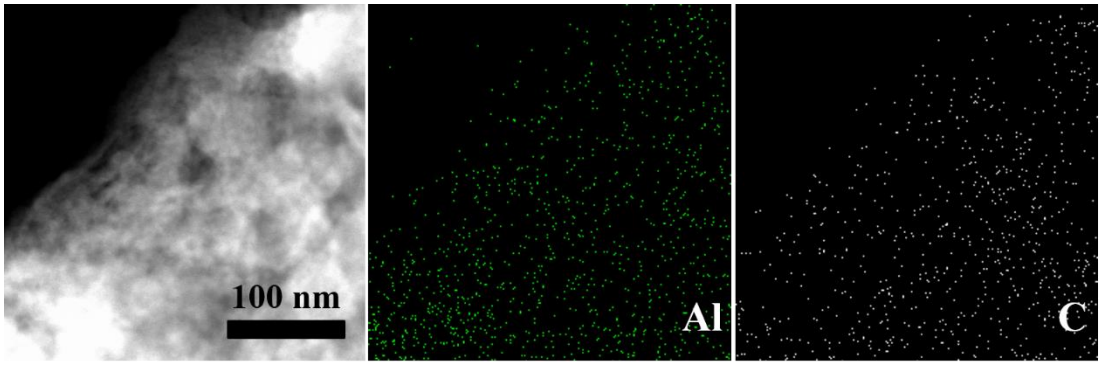

Figure S23 Scanning TEM (STEM) image and the corresponding element mapping of mp-Al@G electrode after 100 cycles at a current density of 0.5 A g^{-1}.

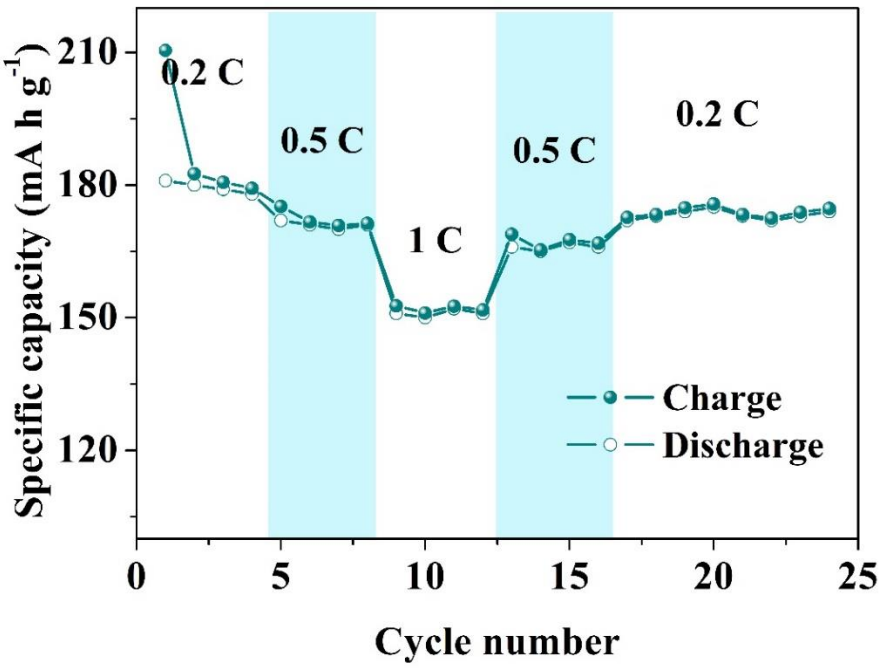

Figure S24 Rate performance of NCM electrode in half cells.

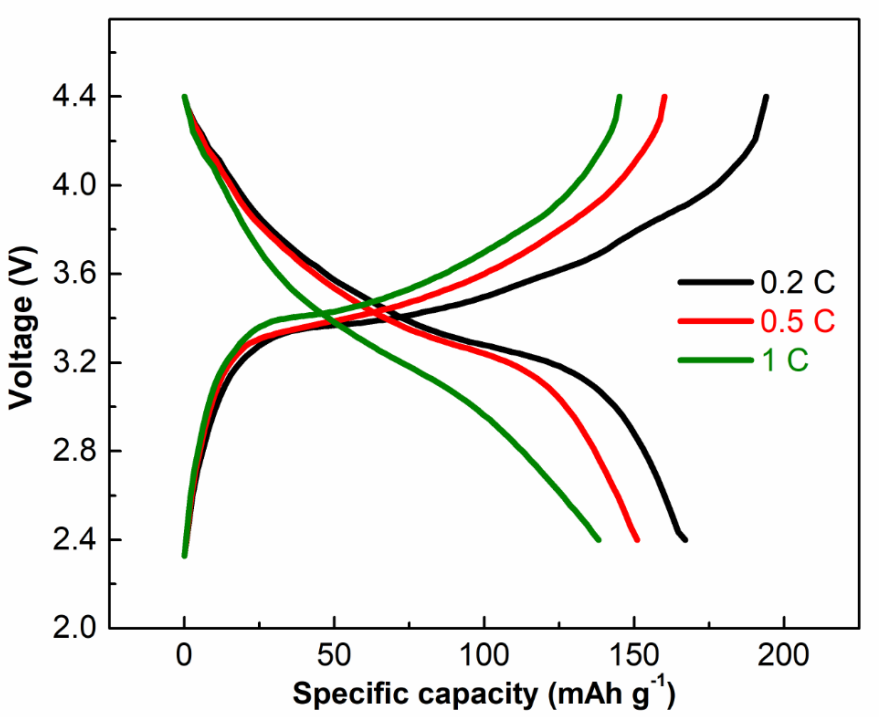

Figure S25 Galvanostatic charge-discharge curves of mp-Al@G//NCM full cells at 0.2 C, 0.5 C, and 1 C, respectively.

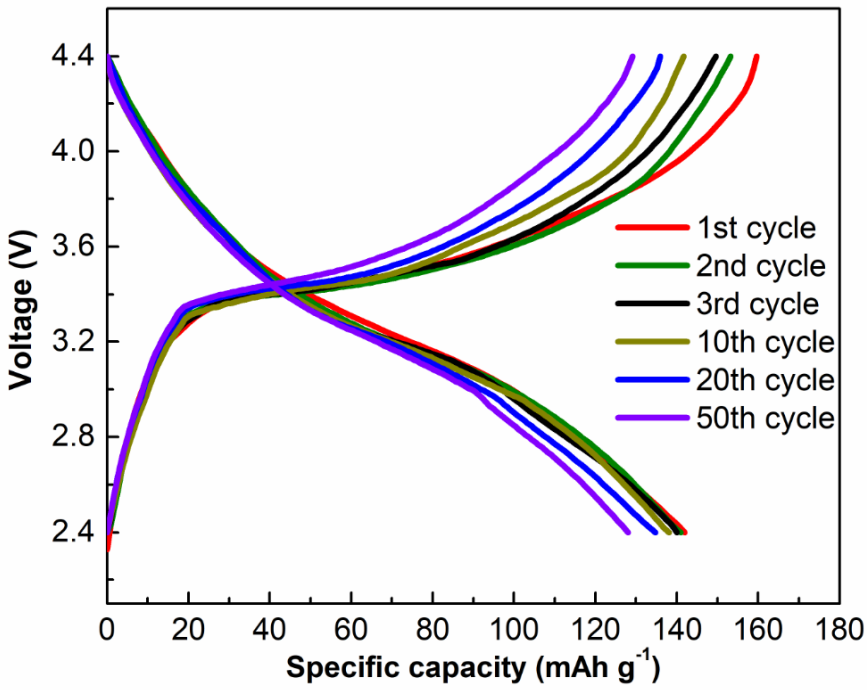

Figure S26 Galvanostatic charge-discharge curves of mp-Al@G//NCM full cells for the 1st, 2nd, 3rd, 10th, 20th, and 50th cycle at 1 C.

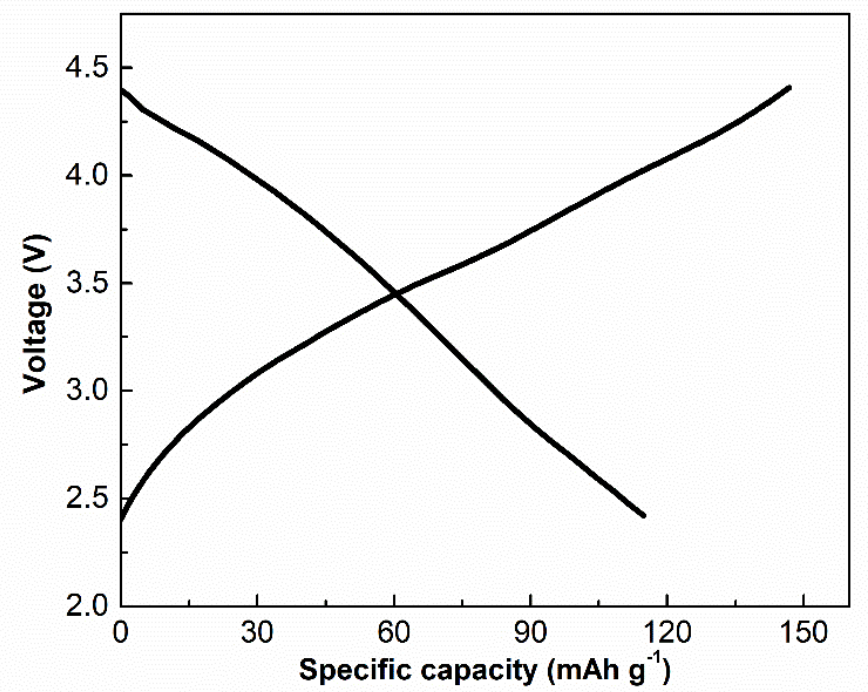

Figure S27 Voltage profiles of graphene//NCM full cells of the first cycle at 1 C. The specific capacity was calculated based on the total weight of anode and cathode materials.

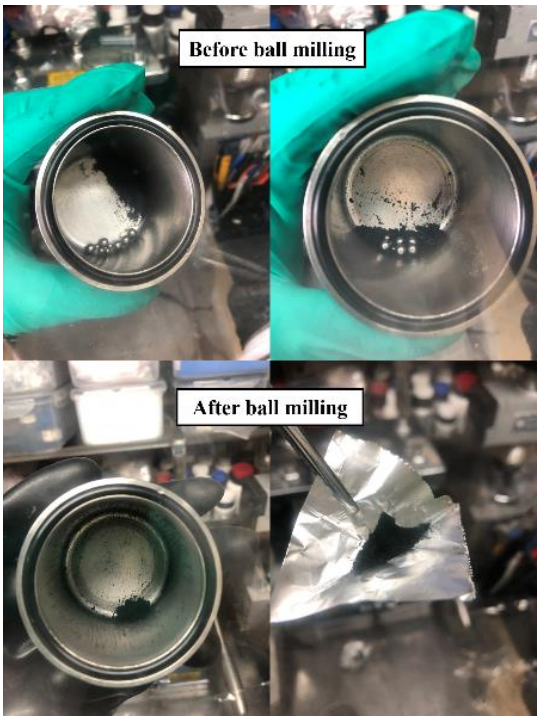

Figure S28 The digital photos of the ball-milled composite of Mg@G and anhydrous $AlCl_3$ before and after the milling process.

Table S1. Comparison of the electrochemical performance of the as-synthesized mp-Al@G with some selected alloying-based anode materials in LIBs. OMC: ordered mesoporous carbon; CNT: carbon nanotube; MWCNT: multi-walled CNT.

Materials	Current density	Reversible specific capacity	Reference
polymer coated Si/C	0.1 A g^{-1}	722 mA h g^{-1} after 100 cycles	[8]
Si@C-rGO	0.3 A g^{-1}	900 mA h g^{-1} after 400 cycles	[9]
Si@SiOx/C	0.21 A g^{-1}	783 mA h g^{-1} after 300 cycles	[10]
Porous Si/C	0.1 A g^{-1}	531 mA h g^{-1} after 200 cycles	[11]
Si/C	0.2 A g^{-1}	952 mA h g^{-1} after 50 cycles	[12]
Si-CNTs	0.5 A g^{-1}	1031 mA h g^{-1} after 100 cycles	[13]
Si/C granules	0.45 A g^{-1}	376 mA h g^{-1} after 300 cycles	[14]
Si/C Microspheres	0.3 A g^{-1}	466 mA h g^{-1} after 500 cycles	[15]
Si@SiO_2@C	0.1 A g^{-1}	920 mA h g^{-1} after 100 cycles	[16]
Si-granadillas	0.25 A g^{-1}	1080 mA h g^{-1} after 200 cycles	[17]
graphene-scaffolded Si/graphite	0.37 A g^{-1}	445 mA h g^{-1} after 300 cycles	[18]
Sn/graphene	0.1 A g^{-1}	805 mA h g^{-1} after 200 cycles	[19]
Sn-C	0.1 A g^{-1}	450 mA h g^{-1} after 100 cycles	[20]
Sn/C	0.2 A g^{-1}	722 mA h g^{-1} after 100 cycles	[21]
Ge/ GeO_2−OMC	0.2 A g^{-1}	824 mA h g^{-1} after 100 cycles	[22]
Ge@C	0.5 A g^{-1}	800 mA h g^{-1} after 600 cycles	[23]
Ge@N-CNTs	0.1 A g^{-1}	892 mA h g^{-1} after 200 cycles	[24]
Al layers-graphene	0.03 A g^{-1}	308 mA h g^{-1} after 50 cycles	[25]
Al/rGO	0.5 A g^{-1}	998 mA h g^{-1} after 500 cycles	[26]
Al/MoS_2/C	0.1 A g^{-1}	451 mA h g^{-1} after 40 cycles	[27]
Al@Ni/MWCNTs	0.2 A g^{-1}	401 mA h g^{-1} after 50 cycles	[28]
Al@C/Expanded Graphite	0.05 A g^{-1}	657 mA h g^{-1} after 50 cycles	[29]
mp-Al@G	0.2 A g^{-1}	1020 mA h g^{-1} after 100 cycles	This work

Table S2. The corresponding fitting values based on the equivalent circuit.

Materials	Cycles	R_S (Ω)	R_{SEI} (Ω)	R_{ct} (Ω)	CPE_1 (μF)	CPE_2 (mF)
mp-Al@G	1	2.5	10.2	112.7	31.5	0.8
	100	5.8	16.4	130.3	85.0	2.2
BM Al-G	1	2.9	35.3	138.5	58.3	1.3
	100	3.1	54.4	188.5	24.3	1.8

References:

1 D. Chao, C. Zhu, P. Yang, X. Xia, J. Liu, J. Wang, X. Fan, S. V. Savilov, J. Lin, H. J. Fan and Z. X. Shen, *Nat. Commun.*, 2016, **7**, 12122.

2 T. Brezesinski, J. Wang, S. H. Tolbert and B. Dunn, *Nat. Mater.*, 2010, **9**, 146-151.

3 V. Augustyn, P. Simon and B. Dunn, *Energy Environ. Sci.*, 2014, **7**, 1597-1614.

4 Y. Huang, G. Xia, J. Chen, B. Zhang, Q. Li and X. Yu, *Prog. Nat. Sci.*, 2017, **27**, 87-93.

5 H. J. Kim, S. Choi, S. J. Lee, M. W. Seo, J. G. Lee, E. Deniz, Y. J. Lee, E. K. Kim and J. W. Choi, *Nano Lett.*, 2016, **16**, 282-288.

6 Z. Liu, S. Bai, B. Liu, P. Guo, M. Lv, D. Liu and D. He, *J. Mater. Chem. A*, 2017, **5**, 13168-13175.

7 R. J. C. Dubey, J. Nüssli, L. Piveteau, K. V. Kravchyk, M. D. Rossell, M. Campanini, R. Erni, M. V. Kovalenko and N. P. Stadie, *ACS Appl. Mater. Interfaces*, 2019, DOI: 10.1021/acsami.9b03886.

8 Y. Sun, J. Lopez, H.-W. Lee, N. Liu, G. Zheng, C.-L. Wu, J. Sun, W. Liu, J. W. Chung, Z. Bao and Y. Cui, *Adv. Mater.*, 2016, **28**, 2455-2461.

9 D. A. Agyeman, K. Song, G.-H. Lee, M. Park and Y.-M. Kang, *Adv. Energy Mater.*, 2016, **6**, 1600904.

10 G. Zheng, Y. Xiang, L. Xu, H. Luo, B. Wang, Y. Liu, X. Han, W. Zhao, S. Chen, H. Chen, Q. Zhang, T. Zhu and Y. Yang, *Adv. Energy Mater.*, 2018, **8**, 1801718.

11 X. Li, P. Yan, X. Xiao, J. H. Woo, C. Wang, J. Liua and J.-G. Zhang, *Energy Environ. Sci.*, 2017, **10**, 1427-1434.

12 H. Tian, X. Tan, F. Xin, C. Wang and W. Han, *Nano Energy*, 2015, **11**, 490-499.

13 Y.-C. Zhang, Y. You, S. Xin, Y.-X. Yin, J. Zhang, P. Wang, X.-S. Zheng, F.-F. Cao and Y.-G. Guo, *Nano Energy*, 2016, **25**, 120-127.

14 Q. Xu, J.-K. Sun, J.-Y. Li, Y.-X. Yin and Y.-G. Guo, *Energy Storage Mater.*, 2018, **12**, 54-60.

15 Q. Xu, J.-Y. Li, J.-K. Sun, Y.-X. Yin, L.-J. Wan and Y.-G. Guo, *Adv. Energy Mater.*, 2017, **7**, 1601481.

16 X. Li, P. Meduri, X. Chen, W. Qi, M. H. Engelhard, W. Xu, F. Ding, J. Xiao, W. Wang, C. Wang, J.-G. Zhang and J. Liu, *J. Mater. Chem.*, 2012, **22**, 11014-11017.

17 L. Zhang, R. Rajagopalan, H. Guo, X. Hu, S. Dou and H. Liu, *Adv. Funct. Mater.*, 2016, **26**, 440-446.

18 S. Zhu, J. Zhou, Y. Guan, W. Cai, Y. Zhao, Y. Zhu, L. Zhu, Y. Zhu and Y. Qian, *Small*, 2018, **14**, 153-157.

19 M. Ma, J. Yan, C. Yu and S. Guo, *J. Phys. Chem. C*, 2018, **122**, 25211-25218.

20 J. Hassoun, G. Derrien, S. Panero and B. Scrosati, *Adv. Mater.*, 2008, **20**, 3169-3175.

21 Z. Zhu, S. Wang, J. Du, Q. Jin, T. Zhang, F. Cheng and J. Chen, *Nano Lett.*, 2014, **14**, 153-157.

22 L. Zeng, X. Huang, X. Chen, C. Zheng, Q. Qian, Q. Chen and M. Wei, *ACS Appl. Mater. Interfaces*, 2016, **8**, 232-239.

23 C. Yue, Z. Liu, W. J. Chang, W. I. Park and T. Song, *Electrochim. Acta*, 2018, **290**, 236-243.

24 H. P. Guo, B. Y. Ruan, L. L. Liu, L. Zhang, Z. L. Tao, S. L. Chou, J. Z. Wang and H. K. Liu, *Small*, 2017, **13**, 1700920.

25 J. Gu, B. Li, Z. Du, C. Zhang, D. Zhang and S. Yang, *Adv. Funct. Mater.*, 2017, **27**, 1700840.

26 X. Chang, Z. Xie, Z. Liu, X. Zheng, J. Zheng and X. Li, *Nano Energy*, 2017, **41**, 731-737.

27 Q.-Y. Li, Q.-C. Pan, G.-H. Yang, X.-L. Lin, Z.-X. Yan, H.-Q. Wang and Y.-G. Huang, *RSC Adv.*, 2015, **5**, 85338-85343.

28 H. Algul, M. Tokur, M. Uysal, T. Cetinkaya, H. Akbulut and A. Alp, *J. Appl. Electrochem.*, 2016, **46**, 735-743.

29 Y. Huang, X. Lin, Q. Pan, Q. Li, X. Zhang, Z. Yan, X. Wu, Z. He and H. Wang, *Electrochim. Acta*, 2016, **193**, 253-260.